Quantum sensor network metrology with bright solitons

Dmitriy Tsarev [1], Stepan Osipov [1], Ray-Kuang Lee [2,3], Sergey Kulik [4,5] and Alexander Alodjants [1,5,*]

[1] Institute of Advansed Data Transfer Systems, ITMO University, Saint Petersburg 197101, Russia
[2] Institute of Photonics Technologies, National Tsing Hua University, Hsinchu 30013, Taiwan
[3] Center for Quantum Science and Technology, Hsinchu 30013, Taiwan
[4] Quantum Technology Centre, Faculty of Physics, M. V. Lomonosov Moscow State University, Moscow 119991, Russia
[5] Quantum Light Engineering Laboratory, Institute of Natural and Exact Sciences, South Ural State University, Chelyabinsk 454080, Russia

(Received 23 May 2023; accepted 16 November 2023; published 13 December 2023)

We consider a multiparameter quantum metrology problem with bright soliton networks in the presence of weak losses. We introduce the general Heisenberg limit (GHL) $\sigma_\chi = 1/N^k$ that characterizes fundamental limitations for unknown parameter measurement and estimation accuracy σ_χ within linear ($k = 1$) and nonlinear ($k = 3$) quantum metrology approaches to solitons. We examine multipartite NOON states specially prepared for the improvement of multiparameter estimation protocols. As a particular example of producing such states, we propose a three-mode soliton Josephson-junction (TMSJJ) model as a three-mode extension for the soliton Josephson-junction bosonic model, which we previously proposed. The energy spectrum of the TMSJJ exhibits sharp phase transition peculiarities for the TMSJJ ground state. The transition occurs from a Gaussian-like (coherent) state to the superposition of entangled Fock states, which rapidly approach the three-mode NOON state. We show that in the presence of weak losses the TMSJJ enables saturation scaling relevant to the optimal state limit close to the GHL. Our findings open prospects for quantum network sensorics with atomtronic circuits.

DOI: 10.1103/PhysRevA.108.062612

I. INTRODUCTION

Quantum metrology and sensorics represent a meaningful practical result of current quantum technologies [1,2]. Real-world quantum metrological applications may be found in fundamental science achievements, navigation and space, geology, life science, ecology and environment, and civil engineering (see, e.g., [3,4]). From the practical point of view, advanced quantum metrology devices and sensors require an interface with networks, which may be inherent to quantum Internet in the near future (see [5]); quantum networks also bring new advantages and opportunities to quantum sensorics [6,7]. In practice, on-chip quantum sensor networks (QSNs) may be implemented by atomtronic [8] or photonic [9–11] circuit facilities. Thus, an urgent current goal is to study the capabilities and fundamental limitations for the measurement and estimation accuracy of distributed quantum sensors.

In the atomic optics domain, high-precision quantum metrology devices operate with atomic Bose-Einstein condensates (BECs) [12], which may be recognized as some analogs of photonic setups [13]. Measurement and estimation of some unknown phase-dependent parameters inherent to atomic systems are primary in this case. It is instructive to mention linear and nonlinear quantum metrology approaches that we examine in this paper.

In the framework of linear quantum metrology, estimated phase ϕ linearly depends on average particle number N, i.e., $\phi = \chi N$, where χ is some unknown parameter that we wish to specify. In nonlinear metrology, we deal with unknown nonlinear phase shift $\phi = \chi N^k$, where $k = 2, 3, \ldots$. In both cases, one can introduce the generalized Heisenberg limit (GHL)

$$\sigma_{\rm GHL}^{(k)} \geqslant \frac{1}{N^k}, \tag{1}$$

that establishes fundamental ultimate accuracy $\sigma_{\rm GHL}^{(k)}$ of one, χ, parameter measurement and estimation.

Thus, familiar linear quantum metrology operates within the Heisenberg limit (HL) obtained from (1) at $k = 1$. Noteworthy, the HL may be saturated by various measurement and/or detection procedures. For example, a two-mode Mach-Zehnder interferometer fed by the ideal NOON state allows a two-mode measurement procedure saturating the HL (see, e.g., [14]). The detection procedure to achieve the HL may be realized in the framework of parity-measurement detection schemes [15,16]. On the other hand, as we showed in [17], it is possible to establish a positive operator-valued measurement (POVM) procedure that enables us to saturate the HL; in general, an n-level quantum system provides at least n^2 POVM elements. Theoretical studies of POVM peculiarities in high-dimension systems have been performed in a number of works [18–23]. Quantum measurements established by symmetric-informationally-complete (SIC) POVMs are optimal for quantum state tomography and were proposed in systems of various dimensions (see [24–27]). SIC POVMs were verified experimentally for photonic low-dimension schemes including photonic circuits and spontaneous down

*alexander_ap@list.ru

conversion processes (see, e.g., [28–32]). These schemes are described by discrete variables. However, in this paper, we consider a mesoscopic number of particles that requires a continuous variable approach. In this limit, SIC POVM methods represent a great interest and are applicable, at least in theory (see [17]). However, the experimental verification of SIC POVMs operating in a high-dimension system currently looks quite cumbersome. To be more specific, in this paper, we analyze the NOON state formation for mesoscopic atomic systems described by continuous variables.

From a practical point of view, Eq. (1) implies phase super-resolution that we can achieve within the N-particle interference. In this sense, Eq. (1) helps to recognize phase super-sensitivity that may be verified by the parameter (see [33])

$$\mathcal{S} = \frac{1}{\sqrt{\nu N}\sigma_\chi}, \tag{2}$$

where ν is the number of trials (measurements), and we set it equal to 1 for simplicity; σ_χ represents the accuracy attainable for the χ parameter measurement and estimation. Establishing the quantum Cramér-Rao (QCR) bound for σ_χ from (2) we obtain

$$0 \leqslant \mathcal{S} \leqslant \sqrt{\frac{F}{N}}, \tag{3}$$

where F is the Fisher information related to the χ parameter measurement and estimation. Notably, if we apply inequality (1) to Eqs. (2) and (3), we can obtain

$$0 \leqslant \mathcal{S} \leqslant N^{k-1/2}. \tag{4}$$

The right part in Eq. (4) establishes the upper bound for phase resolution performed by a quantum sensor. In the classical domain, $\mathcal{S}$ obeys inequalities

$$0 \leqslant \mathcal{S}_{\rm cl} \leqslant 1, \tag{5}$$

that may be achieved in the framework of the linear metrology ($k = 1$) approach with coherent (Glauber) states. As it follows from (3)–(5), purely quantum sensitivity for $\mathcal{S}$, that is $\mathcal{S}_q \equiv \mathcal{S} > 1$, requires achievement of quantum Fisher information (QFI) F beyond value $F \simeq \sqrt{N}$, which is relevant to the standard quantum limit (SQL) of phase estimation.

At $k > 1$, Eq. (1) defines the super-Heisenberg limit (SHL) that enables determination of the ultimate accuracy of unknown parameter measurement and estimation within the nonlinear quantum metrology. In this case, the HL can be overcome even with Glauber's coherent states due to nonlinearity [34]. It is shown that the two-mode NOON state can saturate the SHL with $k = 2$ within an unknown nonlinear phase shift estimation procedure. The SHL implies the use of squeezing and nonlinear properties of the atomic system (see [35]).

Previously, in [36], we showed that quantum bright solitons provide the maximal value of degree $k = 3$ that may be obtained with a Kerr-like medium due to soliton spatial degrees of freedom. At the same time, we proposed the soliton Josephson-junction (SJJ) device, which enables us to produce Fock state superposition close to NOON states and protected against losses of a small number of particles [37]. It is important to stress that NOON as well as "superentangled" states may be achieved with weakly attracting particles, which correspond to negative scattering length (see [38,39]).

Recently, fundamental aspects of multiparameter sensorics and metrology have become the subject of intensive study [40,41]. Various measurement strategies and procedures are discussed within simple two-mode phase estimation schemes [42,43]. The capacity of nonclassical states aimed at improvement of overall metrological accuracy achieved within QSNs represents a primary task that has not been fully studied yet (see, e.g., [44,45]).

In this paper, we continue our studies on quantum metrology with solitons, established within the two-mode approach [16,17,36,37,46,47]. In [16,36,37,46], we discussed in detail atomic BECs possessing negative scattering length as a physical platform for metrology and SJJ realization in practice (see [48]). The influence of losses and decoherence was analyzed in [37,46,47].

The paper is arranged as follows. In Sec. II, we analyze the fundamental limits for multimode (multiparameter) nonlinear quantum metrology with quantum solitons spatially distributed within some QSN and established in Fig. 1(a). We specify some peculiarities for parameter accuracy estimation resulting from the implementation of the spatially distributed multipartite NOON state. Then, we examine the multiparameter metrology and sensing task in the practically important two-parameter quantum metrology limit. In Sec. III, we give a general description of a three-mode soliton Josephson-junction (TMSJJ) model for metrological applications. We show how to obtain a three-mode NOON-like (entangled Fock) state by coupled bright solitons containing a mesoscopic number of particles. First, we discuss a semiclassical TMSJJ model for atomic BECs trapped in a symmetric three-well potential. The geometry of the TMSJJ is presented in Fig. 1(b). To be more specific, we analyze a completely symmetric case of soliton couplings (see [49–51]). Second, for the full-quantum TMSJJ model we examine the energy spectrum exhibiting a phase transition to an entangled Fock state that anticipates three-mode NOON state formation. In Sec. IV, we combine these results accounting for losses that eventually occur in the metrological scheme during quantum state evolution [see Fig. 1(a)]. We examine a complete three-mode soliton metrology task that includes the three-mode NOON state preparation, phase accumulation, and measurement procedure. The multiparameter estimation bounds with quantum solitons in the presence of losses are elucidated using the upper bound of Fisher information. We show that in the framework of linear and nonlinear metrologies, the TMSJJ allows approaching the GHL even with weak particle losses. In the Conclusion, we summarize the results obtained.

II. FUNDAMENTAL LIMITS OF MULTIPARAMETER NONLINEAR QUANTUM METROLOGY

Consider the measurement and estimation procedure for a set of unknown parameters χ_j, shown in Fig. 1(a), and exploiting the $(n = d + 1)$-partite $[(d + 1)$-mode$]$ spatially entangled NOON state that we establish as

$$|\psi_{\rm in}\rangle = \varepsilon(|0, N, 0, \dots, 0\rangle + |0, 0, N, \dots, 0\rangle + \dots + |0, 0, 0, \dots, N\rangle) + \sqrt{1-\varepsilon^2 d}|N, 0, 0, \dots 0\rangle, \tag{6}$$

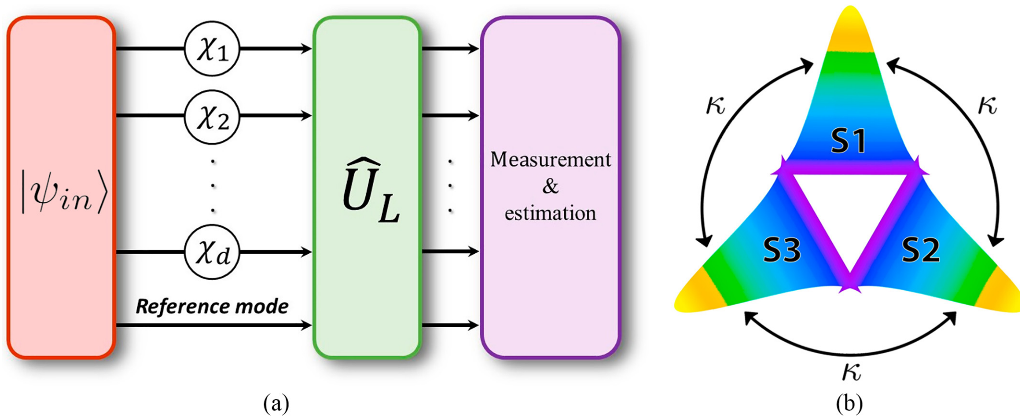

FIG. 1. (a) Sketch of multiparameter quantum metrology circuit with solitons. $|\psi_{\rm in}\rangle$ is a multipartite state of quantum solitons prepared for metrological tasks. This state distributes within the QSN and accumulates phases ϕ_j containing information about estimated parameters χ_j $(j = 1, \dots, d)$. Operator $\hat{U}_L$ denotes the action of a network beam splitter that allows us to build a measurement procedure of unknown parameters with their estimation. Other details are given in the text. (b) Solitons layout for balanced tripartite NOON state preparation. The solitons are trapped in a three-well potential (not shown) providing each-to-each tunnel coupling. The symmetry of the system indicates invariance under cyclic permutation of phase and particle difference variables, respectively. The double-sided arrows illustrate tunnel couplings between the solitons.

where $\varepsilon \neq 0$ describes the amplitude of the estimated channels in Fig. 1(a). Then, assume that the $|\psi_{\rm in}\rangle$ state is distributed over the QSN nodes accumulating unknown phase shifts $\phi_j = \chi_j N^k$, $j = 1, \dots, d$. Thus, after transforming $|\psi_{\rm in}\rangle$, we obtain

$$|\psi_n\rangle = \varepsilon(e^{i\phi_1}|0, N, 0, \dots, 0\rangle + e^{i\phi_2}|0, 0, N, \dots, 0\rangle + \dots + e^{i\phi_d}|0, 0, 0, \dots, N\rangle) + \sqrt{1-\varepsilon^2 d}|N, 0, 0, \dots, 0\rangle. \tag{7}$$

The QSN capacity corresponds to state $|\psi_n\rangle$ and consists of simultaneous estimation up to d phase parameters χ_j in respect of the reference mode [the last term in (7)].

Equation (7) with $k = 1$ corresponds to the linear metrology approach, while $k > 1$, $k \in \boldsymbol{N}$, establishes the nonlinear quantum metrology limit. Particularly, $k = 2$, if we use routine Kerr-like media for unknown phase shifts in Fig. 1(a) and plane-wave description (see [34]). For nonlinear quantum metrology with a soliton network, we can take $k = 3$ (see [37]).

In the framework of multiparameter quantum metrology, we are interested in minimizing the overall variance

$$\sigma_{\boldsymbol{\chi}} \equiv \left(\sum_{i=1}^{d} \sigma_{\chi_j}^2\right)^{1/2}, \tag{8}$$

where $\boldsymbol{\chi} \equiv \{\chi_j\}$ denotes a set of unknown parameters, and σ_{χ_j} is an accuracy of their simultaneous measurement and estimation that we characterize by QFI. In a general case of multiparameter estimation, the QFI, $\hat{F}$, represents a $d \times d$ matrix, where d is the number of the parameters to be simultaneously estimated (see [41]). The QFI matrix elements take the form

$$F_{ij} = 4{\rm Re}[\langle\partial_{\chi_i}\psi_n|\partial_{\chi_j}\psi_n\rangle - \langle\partial_{\chi_i}\psi_n|\psi_n\rangle\langle\psi_n|\partial_{\chi_j}\psi_n\rangle], \tag{9}$$

where $|\psi_n\rangle$ is some n-mode state with $n \geqslant d+1$; $\chi_{i,j}$ are measurables, some phase parameters depending on N; $|\partial_{\chi_{i,j}}\psi_n\rangle \equiv \frac{\partial}{\partial\chi_{i,j}}|\psi_n\rangle$. The measurement (overall) accuracy is limited by the QCR bound, which for $\hat{F} = \{F_{ij}\}$ is

$$\sigma_{\boldsymbol{\chi}} \geqslant [{\rm Tr}(\hat{F}^{-1})]^{1/2}. \tag{10}$$

Substituting (7) into (9) we obtain

$$F_{ij} = 4N^{2k}\varepsilon^2(\delta_{ij} - \varepsilon^2), \tag{11}$$

which gives ${\rm Tr}(\hat{F}^{-1}) = \frac{1}{N^{2k}}\frac{d(1+\varepsilon^2-d\varepsilon^2)}{4\varepsilon^2}(1-d\varepsilon^2)$.

Thus, for the balanced NOON state with $\varepsilon = 1/\sqrt{d+1}$ we obtain

$$\sigma_{\boldsymbol{\chi}} \geqslant \frac{1}{N^k}\sqrt{\frac{d(d+1)}{2}}. \tag{12}$$

In particular, for the two-mode NOON state metrology we must take $d = 1$, and (12) leads to the GHL established in (1).

At $d > 1$ the overall accuracy $\sigma_{\boldsymbol{\chi}}$ degrades, and one can obtain $\sigma_{\boldsymbol{\chi}} > \sigma_{\rm GHL}^{(k)}$. For the three-mode NOON state metrology, that we examine below, $d = 2$, the ultimate precision is $\sqrt{3}\sigma_{\rm GHL}^{(k)}$, obtained for the balanced NOON state at $\varepsilon = 1/\sqrt{3}$ [see (7)]. This limit we can overcome with nonbalanced NOON state setting $\varepsilon = 1/\sqrt{d+\sqrt{d}}$ in (7) (see [44]):

$$\sigma_{\boldsymbol{\chi}} \geqslant \frac{1}{N^k}\frac{\sqrt{d}(\sqrt{d}+1)}{2}, \tag{13}$$

which for $d = 2$ approaches $\sigma_{\boldsymbol{\chi}} \geqslant (1 + 1/\sqrt{2})\sigma_{\rm GHL}^{(k)} \simeq \sqrt{2.914}\sigma_{\rm GHL}^{(k)}$, that gives a small advantage in comparison with the balanced NOON state, and the preparation of such optimized states (OSs) is even more complicated. Further, we refer to $\sigma_{\rm OS}^{(k)} = \sqrt{2.914}\sigma_{\rm GHL}^{(k)}$ as the NOON OS limit, while the main focus is made on the NOON-state-based metrology.

III. TMSJJ MODEL FOR TRIPARTITE NOON STATE PREPARATION

A. Semiclassical TMSJJ model

The preparation of state (6) and/or (7) for arbitrary large d represents a nontrivial practical task. In this paper, we examine a realistic situation of quantum metrology with the TMSJJ ($n = 3$) that enables us to prepare $|\psi_{\rm in}\rangle$ or $|\psi_n\rangle$ close to the tripartite NOON state [see (6) and (7)].

Below, we examine the possibility of realizing quantum metrology and sensing with atomic TMSJJ, which is shown in Fig. 1(b) and provides the preparation of states $|\psi_{\rm in}\rangle$ and $|\psi_n\rangle$, respectively (see [37]).

Consider the Hartree (variational) approach to the TMSJJ that represents a generalization of the two-component SJJ (see [16,36]). In Fig. 1(b) we establish the geometry of arranged solitons. The Hamiltonian in the second quantization form may be written as (see [16,17,52])

$$\hat{H} = \sum_{j=1}^{3} \hat{a}_j^\dagger \left(-\frac{1}{2}\frac{\partial^2}{\partial x^2} - \frac{u}{2}\hat{a}_j^\dagger \hat{a}_j \right) \hat{a}_j - \kappa \sum_{j=1}^{3} \sum_{i\neq j} \hat{a}_i^\dagger \hat{a}_j, \quad (14)$$

where $\hat{a}_j \equiv \hat{a}_j(x)$ is the bosonic annihilation operator obeying commutation rule $[\hat{a}_i(x), \hat{a}_j^\dagger(x')] = \delta_{i,j}\delta(x-x')$. In particular, in atomtronics we can assume that condensates are placed within three symmetrically arranged cigar-shaped each-to-each coupled traps, as shown in Fig. 1(b). The nonlinear particle interaction parameter, $u = 2\pi|a_{\rm sc}|/r_0$, is responsible for Kerr-like nonlinearity [52]; $r_0 = \sqrt{\hbar/M\omega_0}$ is the characteristic trap scale in the transverse direction; M is the particle mass; ω_0 is the characteristic harmonic trap frequency; $a_{\rm sc}$ is the BEC particle scattering length. For bright matter solitons, we consider a BEC of attractive particles, such as ^{7}Li, for which $a_{\rm sc} < 0$. We take tunneling coupling constant κ the same for all coupling links between the solitons. The variational state for the system in Fig. 1(b) we chose as [53–55]

$$|\Psi_N\rangle = \frac{1}{\sqrt{N!}} \left[\int_{-\infty}^{\infty} [\psi_1(x)\hat{a}_1^\dagger(x) + \psi_2(x)\hat{a}_2^\dagger(x) + \psi_3(x)\hat{a}_3^\dagger(x)] dx \right]^N |0\rangle, \quad (15)$$

where $|0\rangle \equiv |0_1, 0_2, 0_3\rangle$ denotes the three-mode vacuum state; N is the total number of particles; $\psi_j(x)$ ($j = 1, 2, 3$) is the unknown variational function obeying the normalization condition

$$\sum_{j=1}^{3} \int_{-\infty}^{\infty} |\psi_j(x)|^2 dx = \sum_{j=1}^{3} \frac{N_j}{N} \equiv \sum_{j=1}^{3} n_j = 1, \quad (16)$$

where $0 \leqslant n_j \leqslant 1$ is the fraction of particles populating the jth well. Bosonic creation and annihilation operators act on total state $|\Psi_N\rangle$ in (15) as follows:

$$\hat{a}_j^\dagger(x)|\Psi_N\rangle = \sqrt{N+1}\psi_j^*(x)|\Psi_{N+1}\rangle,$$
$$\hat{a}_j(x)|\Psi_N\rangle = \sqrt{N}\psi_j(x)|\Psi_{N-1}\rangle. \quad (17)$$

The Hamiltonian function in the Hartree approximation may be obtained from Eq. (14) with Eqs. (15) and (17) and reads as

$$H = \langle\Psi_N|\hat{H}|\Psi_N\rangle = N\sum_j \left(\frac{1}{2}\left|\frac{\partial\psi_j}{\partial x}\right|^2 - \frac{u(N-1)}{2}|\psi_j|^4 - \kappa\sum_{i\neq j}\psi_i^*\psi_j \right). \quad (18)$$

Equation (18) implies coupled Gross-Pitaevskii equations

$$i\dot{\psi}_j = -\frac{1}{2}\frac{\partial^2}{\partial x^2}\psi_j - u(N-1)|\psi_j|^2\psi_j - \kappa\psi_m - \kappa\psi_k,$$
$$j, m, k = 1, 2, 3, \quad m \neq j \neq k. \quad (19)$$

In the limit of the absence of coupling, i.e., at $\kappa = 0$ (condensates are isolated within their traps), Eqs. (19) possess separable bright soliton solutions, which look like

$$\psi_j = n_j \frac{\sqrt{u(N-1)}}{2} \mathrm{sech}\left[\frac{u(N-1)}{2} n_j x \right] e^{i\theta_j}, \quad (20)$$

where $\theta_j = \frac{u^2(N-1)^2 n_j^2}{8} t$ is the jth soliton phase; $j = 1, 2, 3$.

The variational approach presumes that soliton populations n_j and phases θ_j become time dependent if the weak coupling between the solitons is realized, $\kappa \neq 0$. Substituting (20) into (18) and integrating over the space variable we obtain

$$H_{\rm eff} = \frac{1}{N}\int_{-\infty}^{\infty} H dx$$
$$= -2\kappa\sum_j \left(\frac{\Lambda}{3}n_j^3 + \frac{1}{4}\sum_{i\neq j} I_{ij}\cos[\theta_j - \theta_i] \right), \quad (21)$$

where $I_{ij} \equiv n_{ij}(1 - z_{ij}^2)(1 - 0.21 z_{ij}^2)$; $n_{ij} = n_j + n_i$; $z_{ij} = (n_j - n_i)/n_{ij}$ is the population imbalance between the ith and jth solitons; $\Lambda = \frac{u^2(N-1)^2}{16\kappa}$ is the vital parameter that governs TMSJJ various dynamical regimes. Notice, (21) describes the energy of the system per particle.

Equation (21) establishes the TMSJJ model in the Hartree approximation possessing two mutually conjugated sets of variables $\{n_j\}$ and $\{\theta_j\}$. From equations $\frac{\partial n_j}{\partial t} = \frac{\partial H_{\text{eff}}}{\partial \theta_j}$ and $\frac{\partial \theta_j}{\partial t} = -\frac{\partial H_{\text{eff}}}{\partial n_j}$ we obtain

$$\dot{n}_1 = \frac{n_{31}}{2}\left(1 - z_{31}^2\right)\left(1 - 0.21z_{31}^2\right)\sin\left[\Theta_{31}\right] - \frac{n_{12}}{2}\left(1 - z_{12}^2\right)\left(1 - 0.21z_{12}^2\right)\sin\left[\Theta_{12}\right], \tag{22a}$$

$$\dot{\Theta}_{12} = \Lambda n_{12}^2 z_{12} - 2z_{12}\left[1.21 - 0.42z_{12}^2\right]\cos\left[\Theta_{12}\right] + \left(\frac{1}{2}\left(1 - z_{23}^2\right)\left(1 - 0.21z_{23}^2\right) + \frac{2n_3 z_{23}}{n_{23}}\left[1.21 - 0.42z_{23}^2\right]\right)\cos\left[\Theta_{23}\right]$$
$$- \left(\frac{1}{2}\left(1 - z_{31}^2\right)\left(1 - 0.21z_{31}^2\right) - \frac{2n_3 z_{31}}{n_{31}}\left[1.21 - 0.42z_{31}^2\right]\right)\cos\left[\Theta_{31}\right], \tag{22b}$$

where $\Theta_{ij} = \theta_j - \theta_i$ (note that $\sum \Theta_{ij} = 0$); the dots in (22) denote the derivatives with respect to renormalized time $\tau = 2\kappa t$. Equations for the other four variables n_2, n_3, Θ_{23}, and Θ_{31} can be explicitly obtained from (22a) and (22b) with cyclic permutation of indices $i, j = 1, 2, 3$.

We are interested in stationary solution of Eqs. (22) assuming $\dot{n}_j = 0$ and $\dot{\Theta}_{ij} = 0$. In general, these solutions correspond to the entangled Schrödinger-cat-like states, which admit NOON state formation in some limit (see [16]). In this paper, we restrict ourselves by examining a complete set of Eqs. (22) useful for the NOON states.

In particular, let us suppose $n_2 = n_3 = \delta$ and $n_1 = 1 - 2\delta$ ($\delta \to 0$), when all particles may be accumulated in a one soliton state. In this limit Eqs. (22) lead to

$$\cos\left[\Theta_{12}\right] = \cos\left[\Theta_{31}\right] = \frac{\Lambda - 0.5\cos\left[\Theta_{23}\right]}{1.58}. \tag{23}$$

The three-mode quantum metrology scheme, that we consider below, requires one mode to be referenced, leaving us two modes that accumulate phase shifts concerning the reference one. In the paper, we examine two particular cases: these phase-shifted modes are either out of phase or in phase. In particular, for the out-of-phase shifts we take for (23) $\Theta_{12} = \Theta_{31} \equiv \Theta_-$ and $\Theta_{23} = -2\Theta_-$ and obtain for the soliton phase

$$\cos\left[\Theta_-\right] = \sqrt{1.124 + \Lambda} - 0.79 \tag{24}$$

existing only at $\Lambda \leqslant 2.08$.

For the second, in-phase shifts, limit, we take $\Theta_{12} = -\Theta_{31} \equiv \Theta_+$ and $\Theta_{23} = 0$ and obtain another solution

$$\cos\left[\Theta_+\right] = \frac{\Lambda - 0.5}{1.58}, \tag{25}$$

which is also valid for $\Lambda \leqslant 2.08$.

Notice, at $\Lambda = 2.08$ both solutions coincide at $\Theta_\pm = 0$, providing another important special case of the NOON state preparation, which we discuss below.

The stationary solutions of (22) under consideration imply $n_1 \approx 1$ or, similarly, $N_1 \approx N$ and $N_2 \approx N_3 \approx 0$ that form state $|N, 0, 0\rangle$ for the first mode of the three-mode NOON state. In the same manner, we can find solutions for the other, $n_2 \approx 1$ and $n_3 \approx 1$, modes involved in the NOON state. The explicit form of the three-mode NOON state that may be obtained from (15) and (20) and takes into account (23) looks like

$$|N00N\rangle_\pm = \frac{1}{\sqrt{3}}\left(|N, 0, 0\rangle + e^{iN\Theta_\pm}|0, N, 0\rangle + e^{\pm iN\Theta_\pm}|0, 0, N\rangle\right), \tag{26}$$

where $\pm$ subscripts identify the in- and out-of-phase NOON states. In (26) we presume that the first channel of the interferometer is a reference one, setting formally $\theta_1 = 0$.

Thus, we can associate each of states $|N00N\rangle_\pm$ in (26) with state $|\psi_n\rangle$ [see (7)], which may be used in quantum metrology to estimate the parameters embodied in phases $\Theta_\pm$. In this case $\Theta_\pm$ directly relates to unknown parameters χ_j shown in Fig. 1(a).

B. Quantum TMSJJ model

To develop a fully quantum TMSJJ model, it is necessary to quantize effective Hamiltonian (21). The quantization procedure that we use below is similar to the one prescribed in [46].

First, we describe the number of particles populating each of the solitons by operators $\hat{N}_i = \hat{a}_i^\dagger \hat{a}_i$, $i = 1, 2, 3$.

Second, we represent annihilation operators $\hat{a}_i$ as $\hat{a}_i = \sqrt{\hat{N}_i}e^{i\hat{\theta}_i}$ (see [56]). Thus, one can use mapping $2N\sqrt{n_i n_j}\cos[\Theta_{ij}] \to (\hat{a}_i^\dagger \hat{a}_j + \hat{a}_j^\dagger \hat{a}_i)$, $i, j = 1, 2, 3$, $i \neq j$. We also introduce relative atomic population imbalance operator $\hat{z}_{ij} = \frac{\hat{a}_j^\dagger \hat{a}_j - \hat{a}_i^\dagger \hat{a}_i}{\hat{a}_j^\dagger \hat{a}_j + \hat{a}_i^\dagger \hat{a}_i}$ and formally establish $\sqrt{1 - \hat{z}_{ij}^2}$ in the Taylor series form as

$$\sqrt{1 - \hat{z}_{ij}^2} = \sum_{k=0}^{\infty}(-1)^k C_{0.5}^k \hat{z}_{ij}^{2k}, \tag{27}$$

where $C_{0.5}^k = \frac{1}{k!}\prod_{l=0}^{k-1}(0.5 - l)$. Finally, the TMSJJ quantum Hamiltonian in the second quantization form looks like [see (21)]

$$\hat{H}_{\text{TMSJJ}} = 2\kappa\left(-\frac{\Lambda}{3N^3}\sum_i\left(\hat{a}_i^\dagger \hat{a}_i\right)^3 - \frac{1}{8N}\left\{\sum_{i\neq j}\sum_{k=0}^{\infty}(-1)^k C_{0.5}^k\left(1 - 0.21\hat{z}_{ij}^2\right)\left(\hat{a}_i^\dagger \hat{a}_j + \hat{a}_j^\dagger \hat{a}_i\right)\hat{z}_{ij}^{2k} + \text{H.c.}\right\}\right), \tag{28}$$

where H.c. stands for the Hermitian conjugate.

We characterize the tripartite quantum state of coupled solitons without losses in general as

$$|\Psi(\tau)\rangle = \sum_{N_1=0}^{N}\sum_{N_2=0}^{N-N_1} A_{N_1,N_2}(\tau)|N_1, N_2, N_3\rangle, \tag{29}$$

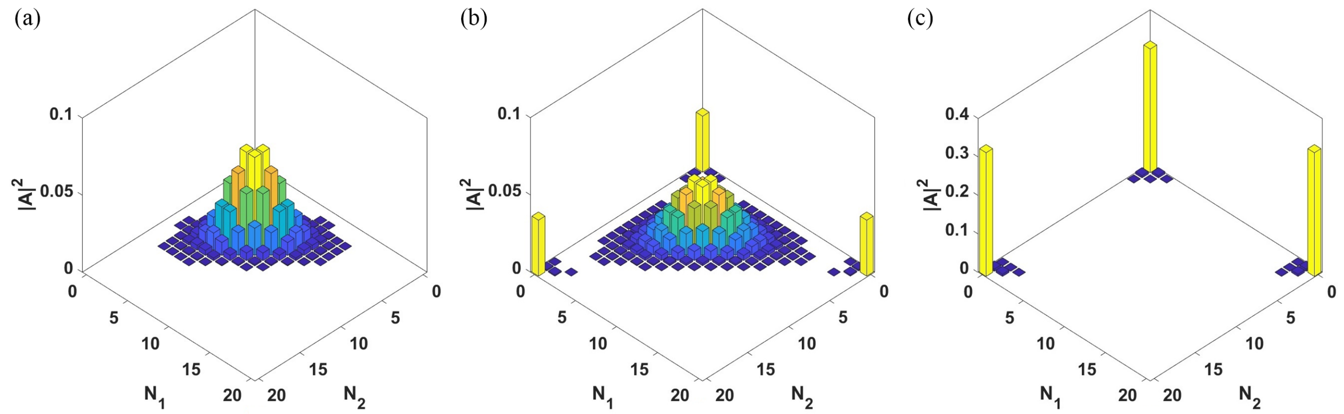

FIG. 2. Distributions for the TMSJJ ground state at (a) $\Lambda = 0$, (b) $\Lambda = \Lambda_{\rm cr} \approx 3.302\,72$, and (c) $\Lambda = 3.305$. $N = 20$.

where $N_1 + N_2 + N_3 = N = \text{const}$; $\tau = 2\kappa t$. Coefficients $A_{N_1,N_2}(\tau)$ in (29) obey Schrödinger equation

$$i\frac{\partial}{\partial \tau}A_{N_1,N_2}(\tau) = \langle N_1, N_2, N_3|\hat{H}_{\rm TMSJJ}|\Psi(\tau)\rangle. \tag{30}$$

Substituting (29) and (28) into (30) we obtain

$$\begin{aligned} i\dot{A}_{N_1,N_2}(\tau) = {}& \alpha_{N_1,N_2}(\Lambda)A_{N_1,N_2} + \beta_{N_1,N_2}A_{N_1-1,N_2+1} + \beta_{N_2,N_1}A_{N_1+1,N_2-1} \\ & + \beta_{N_2,N_3}A_{N_1,N_2-1} + \beta_{N_3,N_2}A_{N_1,N_2+1} + \beta_{N_3,N_1}A_{N_1+1,N_2} + \beta_{N_1,N_3}A_{N_1-1,N_2}, \end{aligned} \tag{31}$$

where we made definitions

$$\alpha_{N_i,N_j} = -\frac{\Lambda}{3}\frac{N_i^3 + N_j^3 + (N - N_i - N_j)^3}{N^3}, \tag{32a}$$

$$\beta_{N_i,N_j} = -\frac{1}{2N}\frac{1}{N_i + N_j}\left((N_j+1)\sqrt{N_i(N_i-1)}\left[1 - 0.21\left(\frac{N_j - N_i}{N_j + N_i}\right)^2\right] + N_i\sqrt{N_j(N_j+1)}\left[1 - 0.21\left(\frac{N_j - N_i + 2}{N_j + N_i}\right)^2\right]\right). \tag{32b}$$

Coefficient $\alpha_{N_i,N_j}(\Lambda)$ corresponds to the energy of the intrawell particle interaction for the TMSJJ system with quantum numbers $N_1 = N_i$, $N_2 = N_j$, and $N_3 = N - N_i - N_j$ at given Λ. The β_{N_i,N_j} coefficient describes the interwell interaction accompanied by tunneling of a single particle from the ith soliton to the jth one.

Hamiltonian (28) is then diagonalized, and one obtains energy eigenvalues E_m, represented in Fig. 3 as a function of tailoring parameter Λ. The ground-state energy of the TMSJJ at $\Lambda < \Lambda_{\rm cr}$ is $E/\kappa N \approx -1.911 - 0.008\Lambda$; it is marked by the solid blue line in Fig. 3. As seen from Fig. 2(a), at $\Lambda < \Lambda_{\rm cr}$ the TMSJJ ground state is a Gaussian-like state that corresponds to the superfluid state of BECs; the particles tend to equally populate all three wells. In Fig. 3 the quantum phase transition is clearly seen to occur at $\Lambda = \Lambda_{\rm cr} \approx 3.302\,72$, similarly to the one in the two-mode SJJ model at $\Lambda \approx 2.000\,992\,5$ (see [46]).

In Fig. 2, we establish the ground-state behavior for the quantum TMSJJ system nearby critical point $\Lambda_{\rm cr}$. In particular, at $\Lambda = \Lambda_{\rm cr}$ the transition to the three-mode entangled Fock state occurs; all N particles tend to populate "edges" $|N_1, 0, 0\rangle$, $|0, N_2, 0\rangle$, and $|0, 0, N_3\rangle$ in the Fock state basis. In this limit, both Gaussian-like and NOON states of the TMSJJ possess the same energy, and, thus, the resulting ground state represents a coherent superposition of them [see Figs. 3 and 2(b)].

At $\Lambda > \Lambda_{\rm cr}$, the NOON state, that is

$$|N00N\rangle = \frac{1}{\sqrt{3}}(|N,0,0\rangle + |0,N,0\rangle + |0,0,N\rangle), \tag{33}$$

becomes energetically favorable for the ground state of solitons [see Fig. 2(c)]. NOON state (33) possesses the energy

$$E = -\kappa N\frac{2\Lambda}{3}, \tag{34}$$

indicated with the lower part of the red dashed line in Fig. 3. Noteworthy, at $\Lambda \leqslant 2.08$ the Hartree approach predicts NOON state (26) that corresponds to some excited levels in Fig. 3. Roughly speaking, the value of the Λ parameter for these states corresponds to the same energy (34) for the upper part of the red dashed line in Fig. 3. Thus, state (33) represents the tripartite NOON state obtained in (26) at $\Theta_\pm = 0$. We will use the NOON state in (33) as a probe one, $|\psi_{\rm in}\rangle$ [see (6)], for two-parameter metrological purposes [see Fig. 1(a)].

The feasibility of achieving $\Lambda_{\rm cr}$ in current experiments with bright solitons is critical for this paper. Notably, usual (two-mode) condensate Josephson junctions, which pose negative scattering length, enable us to obtain the NOON state in

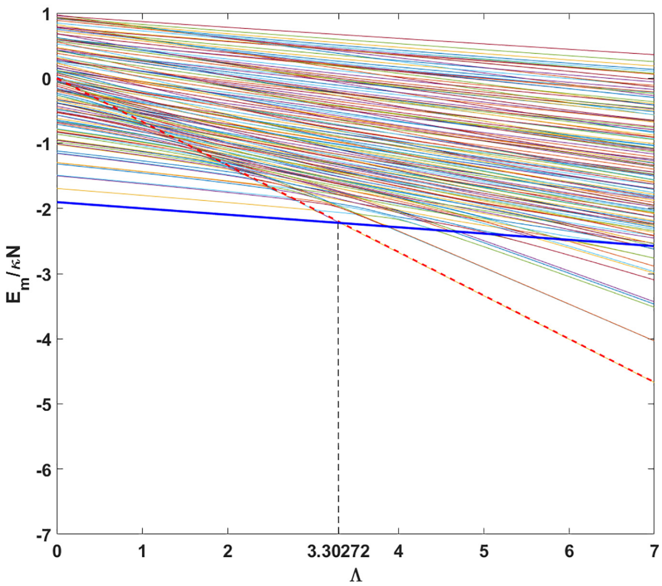

FIG. 3. TMSJJ spectrum as a function of Λ; $N = 20$. The phase transition occurs at $\Lambda_{cr} = 3.302\,72$. The thick blue and dashed red lines denote the energies of atom-coherent and NOON states

the limit of $\Lambda \gg 1$, that implies a large number of particles (see, e.g., [36]). Practically, this limit is hardly achievable with attractive condensate particles due to the condensate wave-function collapse that occurs at $N \simeq 5\times 10^3$ for lithium condensates [48,57]. In contrast, the NOON states based on matter-wave bright solitons may be observed with BEC solitons possessing the mesoscopic number of particles (up to 1000) (see [37,48,57–59]). The value of negative scattering length may be tailored employing the Feshbach resonance technique (see [60]). Thus, critical value Λ_{cr} for the three soliton model may be obtained in the same manner as we previously discussed in [46] for the SJJ system.

Noteworthy, Figs. 2–4, which illustrate the main results in this paper, are plotted for the physically small number of particles $N = 20$ because of lacking computational facilities. Formally, such a number of particles in real-world experiments requires extremely large soliton nonlinearity (see [58]). However, the key physical features we discuss throughout this paper for coupled solitons remain unchanged with N increasing as a parameter. Thus, we expect the obtained results to be valid for the mesoscopic number of particles (up to 1000) when bright solitons are stable and may be formed in condensates with negative scattering length (see [48]).

IV. LOSSY QUANTUM METROLOGY WITH TMSJJ

Here, we examine a practically feasible two-parameter quantum metrology problem with solitons in the presence of losses. We do not consider the case when loss and decoherence occur under the probe (multipartite) state $|\psi_{in}\rangle$ preparation for further metrological implementation [see Fig. 1(a)]. We discussed in detail how atomic condensates are suitable for $|\psi_{in}\rangle$ preparation in the two-mode limit in [46] (see also [17,47]). Below we assume that losses may appear in the scheme during probe state $|\psi_{in}\rangle$ evolution [see Fig. 1(a)]. The metrology protocol consists of three steps. The first one corresponds to three-mode NOON state $|\psi_{in}\rangle = |N00N\rangle$ preparation that may be realized by the TMSJJ device [see (33)]. Then, we assume that two modes accumulate relative phases, that are χ dependent, while one (reference) mode remains unshifted [see Eq. (7)]. Finally, the third step requires some linear operation $\hat{U}_L$ to mix all the modes and make them interfere. For three modes ($n = 3$) we can use a so-called tritter, which is familiar in quantum optics and may be designed by a photonic circuit [61].

We exploit the fictitious beam splitter (FBS) method accounting for particle losses in the scheme in Fig. 1(a). Consider three FBSs, which impose equal transparency parameter $0 < \eta \leqslant 1$; the ideal lossless quantum metrology limit corresponds to value $\eta = 1$. We assume that each FBS acts on a separate channel of the interferometer, transforming the corresponding Fock state as follows (see [62]):

$$|m\rangle \rightarrow \sum_{l=0}^{m} \sqrt{\binom{m}{l} \eta^m (\eta^{-1} - 1)^l}\, |m - l\rangle \otimes |l\rangle, \tag{35}$$

where m is the initial population of the mode; l is the number of particles lost; and $\binom{m}{l} = \frac{m!}{l!(m-l)!}$. Notice, in the optical experiment actual beam splitters can be used to model losses. In this case, the number of particles lost from each mode l_i, $i = 1, 2, 3$, can be measured with photon number resolving detectors.

To be more specific, we consider lossy quantum metrology operating with the input state (29) generated by the TMSJJ. We consider the third mode as the reference one [see Fig. 1(a)]. The other two modes accumulate a relative phase shift described by operator

$$\hat{U}_{PS} = \exp[i\chi_1(\hat{a}_1^\dagger \hat{a}_1)^k + i\chi_2(\hat{a}_2^\dagger \hat{a}_2)^k]. \tag{36}$$

Noteworthy, operator (36) commutes with the Kraus operator that describes the particle losses within the FBS approach. Therefore, it is not important where particles are lost; it may happen before or after the phase accumulation (see [62]).

Since we are not interested in the lost particles, we can trace them out and consider the mixed output quantum state with a density matrix

$$\rho = \sum_{l_1=0}^{N} \sum_{l_2=0}^{N-l_1} \sum_{l_3=0}^{N-l_1-l_2} p_{l_1,l_2,l_3} |\xi_{l_1,l_2,l_3}\rangle\langle\xi_{l_1,l_2,l_3}|, \tag{37a}$$

$$|\xi_{l_1,l_2,l_3}\rangle = \frac{1}{\sqrt{p_{l_1,l_2,l_3}}} \sum_{N_1=l_1}^{N-l_2-l_3} \sum_{N_2=l_2}^{N-N_1-l_3} A_{N_1,N_2} \sqrt{B_{l_1,l_2,l_3}^{N_1,N_2}}\, e^{i\chi_1 N_1^k + i\chi_2 N_2^k} |N_1 - l_1, N_2 - l_2, N_3 - l_3\rangle, \tag{37b}$$

where $N_3 = N - N_1 - N_2$,

$$B^{N_1,N_2}_{l_1,l_2,l_3} = \binom{N_1}{l_1}\binom{N_2}{l_2}\binom{N_3}{l_3}\eta^N(\eta^{-1}-1)^l \tag{38}$$

with $l = l_1 + l_2 + l_3$;

$$p_{l_1,l_2,l_3} = \sum_{N_1=l_1}^{N-l_2-l_3}\sum_{N_2=l_2}^{N-N_1-l_3} |A_{N_1,N_2}|^2 B^{N_1,N_2}_{l_1,l_2,l_3}$$

is the probability to lose exactly l_1, l_2, and l_3 particles from the three interferometer channels.

For the QFI, we restrict ourselves only by its upper bound, $\tilde{F}$, which looks like

$$F_{ij} \leqslant \widetilde{F}_{ij} = 4\sum_{l_1=0}^{N}\sum_{l_2=0}^{N-l_1}\sum_{l_3=0}^{N-l_1-l_2} p_{l_1,l_2,l_3}[\langle\partial_{\chi_i}\xi_{l_1,l_2,l_3}|\partial_{\chi_j}\xi_{l_1,l_2,l_3}\rangle - \langle\partial_{\chi_i}\xi_{l_1,l_2,l_3}|\xi_{l_1,l_2,l_3}\rangle\langle\xi_{l_1,l_2,l_3}|\partial_{\chi_j}\xi_{l_1,l_2,l_3}\rangle]. \tag{39}$$

Substituting (37) into (39) we obtain

$$\begin{aligned}\widetilde{F}_{ij} =& 4\sum_{N_1=0}^{N}\sum_{N_2=0}^{N-N_1}(N_iN_j)^k|A_{N_1,N_2}|^2 \\ &- 4\sum_{l_1=0}^{N}\sum_{l_2=0}^{N-l_1}\sum_{l_3=0}^{N-l_1-l_2}\frac{\left(\sum_{N_1=l_1}^{N-l_2-l_3}\sum_{N_2=l_2}^{N-N_1-l_3}N_i|A_{N_1,N_2}|^2B^{N_1,N_2}_{l_1,l_2,l_3}\right)\left(\sum_{N_1=l_1}^{N-l_2-l_3}\sum_{N_2=l_2}^{N-N_1-l_3}N_j|A_{N_1,N_2}|^2B^{N_1,N_2}_{l_1,l_2,l_3}\right)}{\sum_{N_1=l_1}^{N-l_2-l_3}\sum_{N_2=l_2}^{N-N_1-l_3}|A_{N_1,N_2}|^2B^{N_1,N_2}_{l_1,l_2,l_3}}.\end{aligned} \tag{40}$$

Notice, at $\eta = 1$ (i.e., without particle losses) $B^{N_1,N_2}_{0,0,0} = 1$ and $B^{N_1,N_2}_{l_1,l_2,l_3} = 0$ for any $l_{1,2,3} > 0$. In this case $\tilde{F} = F$.

Coefficients A_{N_1,N_2} can be obtained by numerical simulation of Eqs. (31) and (32) for various Λ. Figure 4 exhibits the principal results of this paper. It demonstrates the capability of the TMSJJ for quantum state preparation, which is relevant to quantum metrology with solitons. In particular, Fig. 4(a) characterizes the linear quantum metrology, while Fig. 4(b) describes the nonlinear quantum metrology approach. We represent the accuracy bound for the χ-parameter measurement and estimation as a function of Λ for different η:

$$\sigma^{(k)} = \left[\mathrm{Tr}\left(\widetilde{\tilde{F}}^{-1}\right)\right]^{1/2}, \tag{41}$$

where $\widetilde{\tilde{F}} \equiv \{\widetilde{F}_{ij}\}$ is the QFI upper bound matrix.

The thick blue curves in Fig. 4 are relevant to the $\eta = 1$ limit, characterizing the maximal metrological capacity that may be achieved without losses in general. In particular, the upper thick blue dashed line characterizes the SQL within

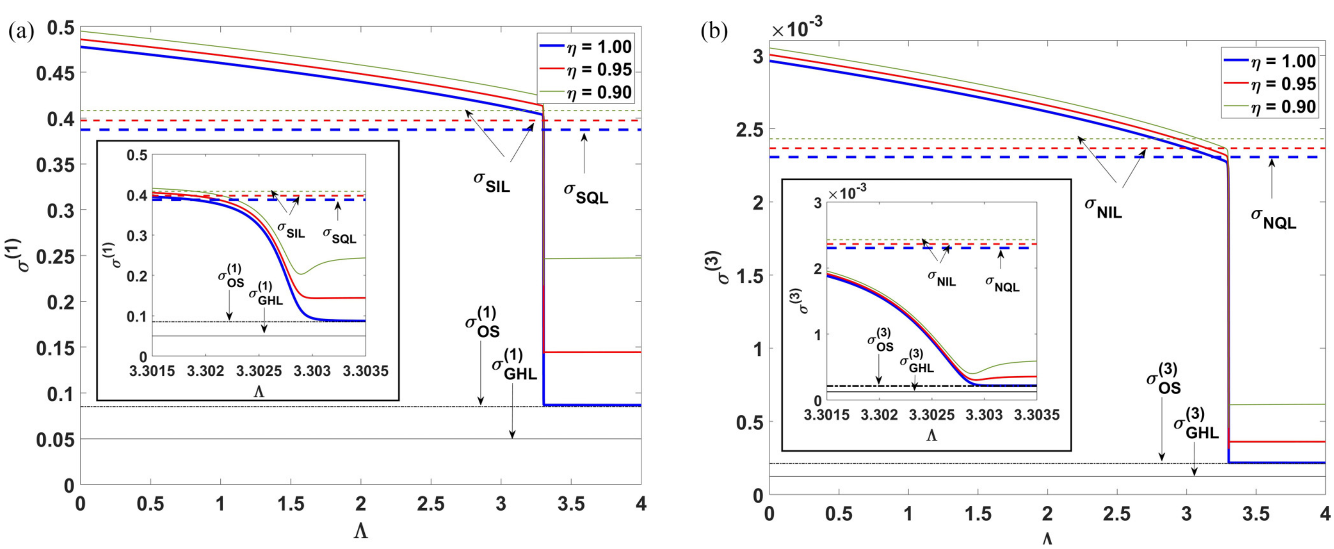

FIG. 4. Accuracy bound $\sigma^{(k)}$ vs vital parameter Λ for (a) linear ($k = 1$) and (b) nonlinear ($k = 3$) quantum metrology protocols with solitons, respectively. The losses are characterized by deviation of the η parameter from unity. The number of particles is $N = 20$. The limiting linear quantum metrology is characterized by SQL($\sigma_{\rm SQL} = \sqrt{3/N}$) and SIL($\sigma_{\rm SIL} = \sqrt{3/\eta N}$), the dashed lines in (a). Nonlinear quantum metrology described by means of NQL ($\sigma_{\rm NQL} \approx \sqrt{27/N^5}$) and NIL ($\sigma_{\rm NIL} \approx \sqrt{27/\eta N^5}$), the dashed lines in (b). In both cases the black dash-dotted lines denote optimized state accuracy $\sigma^{(k)}_{\rm OS} = \sqrt{2.9}/N^k$ and thin solid black lines denote GHL $\sigma^{(k)}_{\rm GHL} = 1/N^k$. The insets demonstrate accuracy bounds $\sigma^{(k)}$ in the vicinity of critical point $\Lambda = \Lambda_{\rm cr}$. Other details are given in the text.

the linear metrology approach, and nonlinear SQL for the nonlinear one. Both of them may be attained with coherent states (see [44]). One can estimate these limits in the case of two-parameter metrology based on Gaussian three-mode quantum state

$$|\psi\rangle = \sum_{N_1=0}^{N}\sum_{N_2=0}^{N-N_1}\sqrt{p(N_1,N_2)}e^{i\chi_1N_1^k+i\chi_2N_2^k} \times |N_1, N_2, N-N_1-N_2\rangle, \tag{42}$$

where

$$p(N_1,N_2) = \frac{9}{2\sqrt{3}\pi N}\exp\left[-\frac{9}{4N}\left(N_1+N_2-\frac{2N}{3}\right)^2 - \frac{3}{4N}(N_1-N_2)^2\right] \tag{43}$$

characterizes the Gaussian distribution function for $N \gg 1$. Equation (43) implies $\sigma_{\rm SQL} = \sqrt{3/N}$ for the linear quantum metrology ($k = 1$) approach, and $\sigma_{\rm NQL} \approx \sqrt{27/N^5}$ for the nonlinear one, $k = 3$.

In the presence of weak losses $\sigma_{\rm SQL}$ and $\sigma_{\rm NQL}$ establish the standard interferometric limit (SIL) and nonlinear interferometric limit (NIL):

$$\sigma_{\rm SIL} = \sqrt{\frac{3}{\eta N}}, \tag{44}$$

$$\sigma_{\rm NIL} \approx \sqrt{\frac{27}{\eta N^5}}. \tag{45}$$

Also in Fig. 4 we focus on the area nearby the critical value $\Lambda_{\rm cr} \approx 3.302\,72$ that corresponds to the phase transition to the NOON state for the TMSJJ; this area is zoomed in the insets to Figs. 4(a) and 4(b), respectively.

Without of losses in general, accuracy $\sigma^{(k)}$ approaches the optimal state level (see the thick blue curves in Fig. 4). Figure 4 clearly demonstrates that accuracy $\sigma^{(k)}$ beats vital classical interferometric limits (44) and (45) for $\Lambda > \Lambda_{\rm cr}$ even in the presence of moderate losses, i.e., when an almost NOON state is prepared by the TMSJJ.

Finally, let us examine the measurement and estimation procedure with states $|N00N\rangle_\pm$ capable for $|\psi_n\rangle$ formation as a result [see (7) and (26)]. We assume that the three-mode NOON state possesses phase shifts $\Theta_\pm$ providing a unique opportunity to estimate parameter $\chi \equiv \Lambda/N^2 \equiv u^2/16\kappa$. Since there is only one χ parameter to be measured effectively, the QFIs may be calculated as

$$F_\pm = 4[{}_\pm\langle\partial_\chi N00N|\partial_\chi N00N\rangle_\pm - |{}_\pm\langle\partial_\chi N00N|N00N\rangle_\pm|^2], \tag{46}$$

where F_+ and F_- are the QFIs for in- and out-of-phase solitons, respectively; $|\partial\chi N00N\rangle_\pm \equiv \frac{\partial}{\partial\chi}|N00N\rangle_\pm = \frac{\partial\Theta_\pm}{\partial\chi}\frac{\partial}{\partial\Theta_\pm}|N00N\rangle_\pm$; $|N00N\rangle_\pm$ is state (26), and phases $\Theta_\pm$ obey (24) and (25).

After some straightforward calculations for the accuracies of the χ parameter measurement and estimation using the in-phase (σ_{χ_+}) and out-of-phase (σ_{χ_-}) solitons configurations, we obtain

$$\sigma_{\chi_+} = 1.58/N^3, \tag{47}$$

$$\sigma_{\chi_-} = 1.22/N^3, \tag{48}$$

respectively. Remarkably, for both cases, accuracy is inversely proportional to N^3 which represents the metrological limit of phase estimation for interacting solitons [see Figs. 4(a) and 4(b)] [16]. Notably, some improvement of accuracy σ_{χ_-} (in comparison with σ_{χ_+}) appears due to the nonlinear soliton phase counteraccumulation (see [63]).

V. CONCLUSION

In this paper, we have considered the d-parameter quantum metrology problem ($d > 1$) with sensor networks operating with bright solitons. The GHL is introduced for both linear and nonlinear quantum metrology tasks. In this framework, we have first examined the multipartite NOON state distributed over QSN. Notably, general strategies, which use multipartite NOON states, demonstrate the $\sqrt{\frac{d(d+1)}{2}}$ times accuracy degradation in the d parameters measurement and estimation problem [see (12)]. Thus, we have shown that the balanced NOON state is not optimal even without losses in this case. However, for the QSNs, which use coupled solitons, with moderate d, the accuracy is close to the fundamental GHL established in this paper. To be more specific, we have considered the TMSJJ model that allows preparation of the tripartite NOON-like (probe) state suitable for the two parameter metrology problem. The TMSJJ represents a generalization of the two-mode soliton Josephson-junction system established for three weakly coupled solitons (see [37]). We have shown that the TMSJJ exhibits the quantum phase transition to the superposition of entangled Fock states capable of the three-mode NOON state formation with a mesoscopic number of particles. The phase transition occurs at some critical value $\Lambda_{\rm cr}$ of dimensionless parameter Λ that may be obtained within the current experiments with weakly coupled atomic condensates. We have shown that beyond the critical value of parameter Λ accuracy $\sigma^{(k)}$ approaches the optimal state even in the presence of weak losses. We have also provided the quantum metrology protocol of the Kerr-like nonlinear χ-parameter measurement and estimation within the in-phase and out-of-phase soliton configurations. It is shown that the best accuracy of the measurement is close to the GHL [see (48)], which we can achieve with the out-of-phase interacting solitons. Our findings open prospects for the problems of spatially distributed quantum sensing and metrology.

ACKNOWLEDGMENT

D.T., S.O., S.K., and A.A. acknowledge the support from the Ministry of Science and Higher Education of the Russian Federation and South Ural State University (Agreement No. 075-15-2022-1116).

[1] L. Pezzè, A. Smerzi, M. K. Oberthaler, R. Schmied, and P. Treutlein, Quantum metrology with nonclassical states of atomic ensembles, Rev. Mod. Phys. **90**, 035005 (2018).

[2] C. L. Degen, F. Reinhard, and P. Cappellaro, Quantum sensing, Rev. Mod. Phys. **89**, 035002 (2017).

[3] S. E. Crawford, R. A. Shugayev, H. P. Paudel, P. Lu, M. Syamlal, P. R. Ohodnicki, B. Chorpening, R. Gentry, and Y. Duan, Quantum sensing for energy applications: Review and perspective, Adv. Quantum Technol. **4**, 2100049 (2021).

[4] K. Bongs, M. Holynski, J. Vovrosh, P. Bouyer, G. Condon, E. Rasel, C. Schubert, W. P. Schleich, and A. Roura, Taking atom interferometric quantum sensors from the laboratory to real-world applications, Nat. Rev. Phys. **1**, 731 (2019).

[5] S. Wehner, D. Elkouss, and R. Hanson, Quantum internet: A vision for the road ahead, Science **362**, eaam9288 (2018).

[6] A. Z. Goldberg, I. Gianani, M. Barbieri, F. Sciarrino, A. M. Steinberg, and N. Spagnolo, Multiphase estimation without a reference mode, Phys. Rev. A **102**, 022230 (2020).

[7] Z. Zhang and Q. Zhuang, Distributed quantum sensing, Quantum Sci. Technol. **6**, 043001 (2021).

[8] L. Amico, M. Boshier, G. Birkl *et al.*, Roadmap on atomtronics: State of the art and perspective featured, AVS Quantum Sci. **3**, 039201 (2021).

[9] F. Flamini, N. Spagnolo, and F. Sciarrino, Photonic quantum information processing: A review, Rep. Prog. Phys. **82**, 016001 (2019).

[10] W. R. Clements, P. C. Humphreys, B. J. Metcalf, W. S. Kolthammer, and I. A. Walmsley, Optimal design for universal multiport interferometers, Optica **3**, 1460 (2016).

[11] S. A. Fldzhyan, M. Yu. Saygin, and S. P. Kulik, Optimal design of error-tolerant reprogrammable multiport interferometers, Opt. Lett. **45**, 2632 (2020).

[12] D. Becker, M. D. Lachmann, S. T. Seidel *et al.*, Space-borne Bose-Einstein condensation for precision interferometry, Nature (London) **562**, 391 (2018).

[13] E. Polino, M. Valeri, N. Spagnolo, and F. Sciarrino, Photonic quantum metrology, AVS Quantum Sci. **2**, 024703 (2020).

[14] J. P. Dowling, Quantum optical metrology-the lowdown on high-N00N states, Contemp. Phys. **49**, 125 (2008).

[15] R. J. Birrittella, P. M. Alsing, and C. C. Gerry, The parity operator: Applications in quantum metrology, AVS Quantum Sci. **3**, 014701 (2021).

[16] D. V. Tsarev, S. M. Arakelian, Y.-L. Chuang, R.-K. Lee, and A. P. Alodjants, Quantum metrology beyond Heisenberg limit with entangled matter wave solitons, Opt. Express **26**, 19583 (2018).

[17] T. V. Ngo, D. V. Tsarev, R.-K. Lee, and A. P. Alodjants, Bose-Einstein condensate soliton qubit states for metrological applications, Sci. Rep. **11**, 19363 (2021).

[18] A. J. Scott and M. Grassl, Symmetric informationally complete positive-operator-valued measures: A new computer study, J. Math. Phys. **51**, 042203 (2010).

[19] M. Planat and Z. Gedik, Magic informationally complete POVMs with permutations, R. Soc. Open Sci. **4**, 170387 (2017).

[20] M. Yoshida and G. Kimura, Construction of general symmetric-informationally-complete-positive-operator-valued measures by using a complete orthogonal basis, Phys. Rev. A **106**, 022408 (2022).

[21] D. F. Pinto, M. S. Zanetti, M. L. W. Basso, and J. Maziero, Simulation of positive operator-valued measures and quantum instruments via quantum state-preparation algorithms, Phys. Rev. A **107**, 022411 (2023).

[22] H. Zhu, SIC POVMs and Clifford groups in prime dimensions, J. Phys. A **43**, 305305 (2010).

[23] J. M. Renes, R. Blume-Kohout, A. J. Scott, and C. M. Caves, Symmetric informationally complete quantum measurements, J. Math. Phys. **45**, 2171 (2004).

[24] A. Czerwinski, Quantum state tomography with informationally complete POVMs generated in the time domain, Quantum Inf. Process. **20**, 105 (2021).

[25] C. Ferrie and R. Blume-Kohout, Minimax quantum tomography: Estimators and relative entropy bounds, Phys. Rev. Lett. **116**, 090407 (2016).

[26] Yu. I. Bogdanov, G. Brida, M. Genovese, S. P. Kulik, E. V. Moreva, and A. P. Shurupov, Statistical estimation of the efficiency of quantum state tomography protocols, Phys. Rev. Lett. **105**, 010404 (2010).

[27] J. S. Lundeen, A. Feito, H. Coldenstrodt-Ronge, K. L. Pregnell, Ch. Silberhorn, T. C. Ralph, J. Eisert, M. B. Plenio, and I. A. Walmsley, Tomography of quantum detectors, Nat. Phys **5**, 27 (2009).

[28] N. Bent, H. Qassim, A. A. Tahir, D. Sych, G. Leuchs, L. L. Sánchez-Soto, E. Karimi, and R. W. Boyd, Experimental realization of quantum tomography of photonic qudits via symmetric informationally complete positive operator-valued measures, Phys. Rev. X **5**, 041006 (2015).

[29] G. N. M. Tabia, Experimental scheme for qubit and qutrit symmetric informationally complete positive operator-valued measurements using multiport devices, Phys. Rev. A **86**, 062107 (2012).

[30] W. M. Pimenta, B. Marques, T. O. Maciel, R. O. Vianna, A. Delgado, C. Saavedra, and S. Pádua, Minimum tomography of two entangled qutrits using local measurements of one-qutrit symmetric informationally complete positive operator-valued measure, Phys. Rev. A **88**, 012112 (2013).

[31] Z. E. D. Medendorp, F. A. Torres-Ruiz, L. K. Shalm, G. N. M. Tabia, C. A. Fuchs, and A. M. Steinberg, Experimental characterization of qutrits using symmetric informationally complete positive operator-valued measurements, Phys. Rev. A **83**, 051801(R) (2011).

[32] A. Ling, K. P. Soh, A. Lamas-Linares, and C. Kurtsiefer, Experimental polarization state tomography using optimal polarimeters, Phys. Rev. A **74**, 022309 (2006).

[33] R. Okamoto, H. F. Hofmann, T. Nagata, J. L. O'Brien, K. Sasaki, and S. Takeuchi, Beating the standard quantum limit: phase super-sensitivity of N-photon interferometers, New J. Phys. **10**, 073033 (2008).

[34] D. Maldonado-Mundo and A. Luis, Metrological resolution and minimum uncertainty states in linear and nonlinear signal detection schemes, Phys. Rev. A **80**, 063811 (2009).

[35] M. Napolitano and M. W. Mitchell, Nonlinear metrology with a quantum interface, New J. Phys. **12**, 093016 (2010).

[36] D. V. Tsarev, T. V. Ngo, R.-K. Lee, and A. P. Alodjants, Nonlinear quantum metrology with moving matter-wave solitons, New J. Phys. **21**, 083041 (2019).

[37] A. P. Alodjants, D. V. Tsarev, T. V. Ngo, and R.-K. Lee, Enhanced nonlinear quantum metrology with weakly coupled solitons in the presence of particle losses, Phys. Rev. A **105**, 012606 (2022).

[38] G. Mazzarella, L. Salasnich, A. Parola, and F. Toigo, Coherence and entanglement in the ground state of a bosonic Josephson junction: From macroscopic Schrödinger cat states to separable Fock states, Phys. Rev. A **83**, 053607 (2011).

[39] Q. Y. He, M. D. Reid, T. G. Vaughan, C. Gross, M. Oberthaler, and P. D. Drummond, Einstein-Podolsky-Rosen entanglement strategies in two-well Bose-Einstein condensates, Phys. Rev. Lett. **106**, 120405 (2011).

[40] J. Liu, X. M. Lu, Z. Sun, and X. Wang, Quantum multiparameter metrology with generalized entangled coherent state, J. Phys. A **49**, 115302 (2016).

[41] M. Gessner, L. Pezzè, and A. Smerzi, Sensitivity bounds for multiparameter quantum metrology, Phys. Rev. Lett. **121**, 130503 (2018).

[42] L. Pezzè, Entanglement-enhanced sensor networks, Nat. Photon. **15**, 74 (2021).

[43] J. Bringewatt, I. Boettcher, P. Niroula, P. Bienias, and A. V. Gorshkov, Protocols for estimating multiple functions with quantum sensor networks: Geometry and performance, Phys. Rev. Res. **3**, 033011 (2021).

[44] P. C. Humphreys, M. Barbieri, A. Datta, and I. A. Walmsley, Quantum enhanced multiple phase estimation, Phys. Rev. Lett. **111**, 070403 (2013).

[45] S. Hong, J. ur Rehman, Y.-S. Kim, Y.-W. Cho, S.-W. Lee, H. Jung, S. Moon, S.-W. Han, and H.-T. Lim, Quantum enhanced multiple-phase estimation with multi-mode N00N states, Nat. Commun. **12**, 5211 (2021).

[46] D. V. Tsarev, A. P. Alodjants, T. V. Ngo, and R.-K. Lee, Mesoscopic quantum superposition states of weakly-coupled matter-wave solitons, New J. Phys. **22**, 113016 (2020).

[47] V. T. Ngo, D. V. Tsarev, and A. P. Alodjants, Coupled solitons for quantum communication and metrology in the presence of particle dissipation, J. Russ. Laser. Res. **42**, 523 (2021).

[48] L. Khaykovich, F. Schreck, G. Ferrari, T. Bourdel, J. Cubizolles, l. D. Carr, Y. Castin, and C. Salomon, Formation of a matter-wave bright soliton, Science **296**, 1290 (2002).

[49] E. Compagno, G. Quesnel, A. Minguzzi, L. Amico, and D. Feinberg, Multimode N00N states in driven atomtronic circuits, Phys. Rev. Res. **2**, 043118 (2020).

[50] K. Nemoto, C. A. Holmes, G. J. Milburn, and W. J. Munro, Quantum dynamics of three coupled atomic Bose-Einstein condensates, Phys. Rev. A **63**, 013604 (2000).

[51] Q. Guo, X. Z. Chen, and B. Wu, Tunneling dynamics and band structures of three weakly coupled Bose-Einstein condensates, Opt. Express **22**, 19234 (2014).

[52] S. Raghavan and G. P. Agrawan, Switching and self-trapping dynamics of Bose-Einstein solitons, J. Mod. Opt. **47**, 1155 (2000).

[53] Y. Lai and H. A. Haus, Quantum theory of solitons in optical fibers. I. Time-dependent Hartree approximation, Phys. Rev. A **40**, 844 (1989).

[54] Y. Lai and H. A. Haus, Quantum theory of solitons in optical fibers. II. Exact solution, Phys. Rev. A **40**, 854 (1989).

[55] A. P. Alodjants and S. M. Arakelian, Quantum chaos and its observation in coupled optical solitons, Zh. Eksp. Teor. Fiz. **107**, 1792 (1995).

[56] G. S. Paraoanu, S. Kohler, F. Sols, and A. J. Leggett, The Josephson plasmon as a Bogoliubov quasiparticle, J. Phys. B **34**, 4689 (2001).

[57] K. E. Strecker, G. B. Partridge, A. G. Truscott, and R. G. Hulet, Formation and propagation of matter-wave soliton trains, Nature (London) **417**, 150 (2002).

[58] P. G. Kevrekidis, D. J. Frantzeskakis, and R. Carretero-González, *Emergent Nonlinear Phenomena in Bose-Einstein Condensates* (Springer-Verlag, Berlin, 2008).

[59] J. H. V. Nguyen, P. Dyke, D. Luo, B. A. Malomed, and R. G. Hulet, Collisions of matter-wave solitons, Nat. Phys. **10**, 918 (2014).

[60] C. Chin, R. Grimm, P. Julienne, and E. Tiesinga, Feshbach resonances in ultracold gases, Rev. Mod. Phys. **82**, 1225 (2010).

[61] N. Spagnolo, L. Aparo, C. Vitelli, A. Crespi, R. Ramponi, R. Osellame, P. Mataloni, and F. Sciarrino, Quantum interferometry with three-dimensional geometry, Sci. Rep. **2**, 862 (2012).

[62] R. Demkowicz-Dobrzanski, U. Dorner, B. J. Smith, J. S. Lundeen, W. Wasilewski, K. Banaszek, and I. A. Walmsley, Quantum phase estimation with lossy interferometers, Phys. Rev. A **80**, 013825 (2009).

[63] M. Jarzyna and R. Demkowicz-Dobrzanski, Quantum interferometry with and without an external phase reference, Phys. Rev. A **85**, 011801(R) (2012).